Commun. Theor. Phys. **72** (2020) 085103 (10pp) https://doi.org/10.1088/1572-9494/ab8a28

Out-of-time-order correlators in the one-dimensional XY model

Jia-Hui Bao[1] **and Cheng-Yong Zhang**[2,3]

[1] Department of Physics and Siyuan Laboratory, Jinan University, Guangzhou 510632, China
[2] School of Physics and Astronomy, Sun Yat-sen University, 2 Daxue Rd., Zhuhai 519082, China

E-mail: baojh5@mail2.sysu.edu.cn and zhangcy@email.jnu.edu.cn

Received 15 January 2020, revised 2 April 2020
Accepted for publication 3 April 2020
Published 20 July 2020

Abstract

We study the behavior of information spreading in the XY model, using out-of-time-order correlators (OTOCs). The effects of anisotropic parameter γ and external magnetic field λ on OTOCs are studied in detail within thermodynamical limits. The universal form which characterizes the wavefront of information spreading still holds in the XY model. The butterfly speed v_B depends on (γ, λ). At a fixed location, the early-time evolution behavior of OTOCs agrees with the results of the Hausdorff–Baker–Campbell expansion. For long-time evolution, OTOCs with local operators decay as for power law t^{-1}, but those with nonlocal operators show different and nontrivial power law behaviors. We also observe temperature dependence for OTOCs when $(\gamma = 0, \lambda = 1)$. At low temperature, the OTOCs with nonlocal operators show divergence over time.

Keywords: out-of-time-order correlators, information spreading, integrable model

(Some figures may appear in colour only in the online journal)

1. Introduction

Chaos is an interesting phenomenon in nature, and has attracted a lot of attention in the fields of condensed matter theory, quantum information theory, and high energy theory. A feature of chaos is the butterfly effect, which characterizes the chaos of a system as $\sim e^{\lambda_L t}$ [1]. The Lyapunov exponent λ_L is unbounded for classical systems. For quantum systems, a conjecture was recently proposed which established a bound $\lambda_L \leqslant 2\pi k_B T/\hbar$ on strong quantum chaos [2]. This new conjecture encouraged further study of chaos as it relates to both high energy theory [3, 4] and condensed matter theory [5–9].

Quantum chaos theory in a quantum many-body system can be characterized by the out-of-time order correlator (OTOC) of the two related operators W and V. Let us consider the following 'commutator function' first.

$$C(l, t) = \frac{1}{2}\langle [W(l, t), V(0)]^{\dagger}[W(l, t), V(0)]\rangle, \qquad (1)$$

here $\langle ...\rangle \equiv \langle e^{-\beta H} ...\rangle / \langle e^{-\beta H}\rangle$ denotes the thermal average at temperature $T = 1/\beta$ and $W(l, t) \equiv e^{iHt} W(l) e^{-iHt}$. l is the position of operator W, H is the Hamiltonian of the system. Assuming operators W and V are both unitary and Hermitian, we can rewrite $C(l, t) = 1 - \mathrm{Re}[F(l, t)]$. Here, $F(l, t) = \langle W(l, t)V(0)W(l, t)V(0)\rangle$ denotes the so-called OTOC for special time ordering. It captures critical information different from the two-point correlation function. The OTOC can also be understood as the measurement of delocalization of spreading operators. It attracts a lot of attention not only because of its richness in terms of theoretical physics, but also because of its feasibility in experiments [10–15].

The behavior of OTOC has several interesting aspects. For example, the early-time behavior of the OTOC can usually be characterized by the Hausdorff–Baker–Campbell (HBC) formula. Around the wavefront of the spreading operators, there is a conjectured universal form describing the ballistic broadening of the OTOC [16, 17]

$$C(l, t) \sim \exp\left(-c\frac{(l - v_B t)^{1+p}}{t^p}\right), \qquad (2)$$

here, c is constant and v_B is the spreading velocity of the butterfly effect, which is decided by setting the velocity-dependent Lyapunov exponents $\lambda_L(v_B) = 0$. p is a coefficient related to models. For instance, $p = 1$ for a random circuit

[3] Author to whom any correspondence should be addressed.

model [18–20], $p = 1/2$ for a non-interacting translation-invariant model [16, 21, 22], $p = 0$ for a Sachdev–Ye–Kitaev (SYK) model [23], and chains of coupled SYK dots at large N [24]. The long-time aspect of OTOC also exhibits interesting behavior, which may reveal important information about how operators saturate bound chaos.

In order to understand how information spreads quantitatively, calculation of the OTOC in different systems, including integrable, or chaotic systems, is an appropriate place to begin. Recently, some work have been done to analyze the OTOC in conformal field theories [25–29], quantum phase transition [30, 31], Luttinger liquids [32], and also lattice integrable models such as the quantum Ising chain [33], the hard-core boson model [21], quadratic fermions [34], the random field XX spin chain [35], and the symmetric Kitaev chain [36]. Scrambling was observed at the critical point of the Ising spin chain. Weak chaos was also witnessed in some models [37].

It is well known that both the quantum Ising model and the XX model can be seen as special cases of the XY model [38]. This contains an anisotropic parameter γ that denotes the difference of components in the x and y direction for coupling of the two nearest neighbours. This feature accords the XY model several nontrivial quantum phase transitions and properties [39]. Therefore, it is interesting to study OTOCs in the XY model in order to learn how operators grow or how information scrambles.

In this paper we focus on the evolution of OTOCs in the XY model. We find that butterfly velocity is dependent on γ and λ, and that the universal form (2) holds for OTOCs in the XY model. We also study the early-time and long-time behavior of OTOCs. While the former is characterized by the HBC formula, the latter displays quite interesting and unusual power law behaviours. Moreover, we observe an interesting temperature dependence in OTOCs in particular cases.

This paper is organized as follows: we introduce the XY model in section 2, including its quantum phase transition, and procedures to diagonalize the Hamiltonian. In section 3, the calculation method of OTOC will be outlined. Next, we will show the exact evolutions of OTOCs with respect to time and location, and extract the information from them. Finally, in section 4 we will briefly discuss these results and conclude.

2. XY model

The XY model is one of the simplest nontrivial integrable models. It demonstrates rich phase diagram, and has the potential to enable the study of new effects. Its Hamiltonian is as follows:

$$H = -\frac{J}{2}\sum_{j=0}^{N-1}\left[\frac{1+\gamma}{2}\sigma_j^x\sigma_{j+1}^x + \frac{1-\gamma}{2}\sigma_j^y\sigma_{j+1}^y + \lambda\sigma_j^z\right], \quad (3)$$

where γ is the anisotropy coefficient describing the difference of interactive strength in the x and y components. λ describes the magnetic field along the z direction. These two parameters

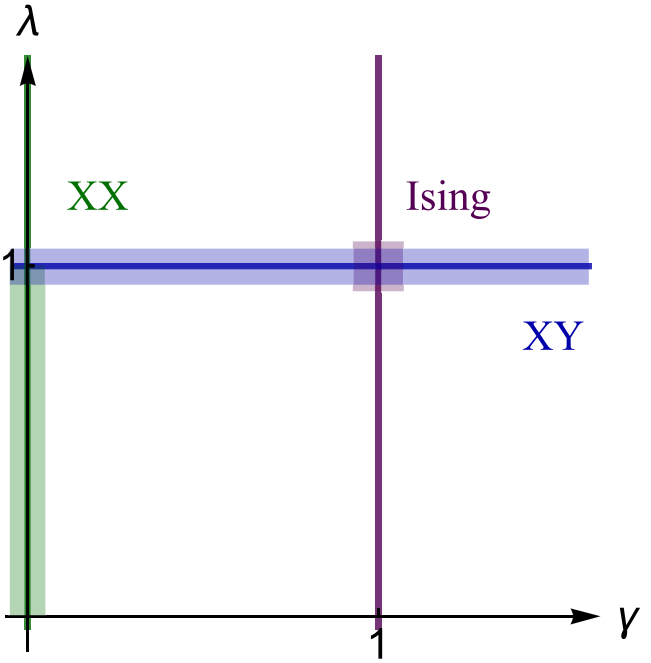

Figure 1. Critical regions of XY model from [41]. Colored shaded areas show the corresponding critical region for each model. We only plot one quadrant due to the existence of symmetry $\gamma \to -\gamma$ and $\lambda \to -\lambda$.

decide the phases and properties of this model. When $\gamma = 0$, it becomes the isotropic XY model (also called XX model). When $\gamma = 1$, it recovers the quantum Ising chain. The relationship between them is shown in figure 1. The shadow areas are the the corresponding critical regions for the different models.

The critical regions at $\lambda = 1$ (blue line) or $\gamma = 0$ (green line) are a conformal invariant, where the spectrum of the theory becomes gapless. They correspond to conformal theories with conformal charge $c = 1/2$ CFT, and $c = 1$ CFT, respectively. The XY chain inculdes two types of quantum phase transition, located at these two lines. The line located at $\lambda = 1$ is a transition from a doubly degenerate state ($\lambda < 1$) to a single ground state ($\lambda > 1$). However, when $(\gamma, \lambda) = (0, 1)$, it is not conformal, since the dynamical critical exponent is two [40].

In order to calculate the OTOC of an XY chain, we should diagonalize its Hamiltonian using the Jordan-Wigner transformation, and the Bogoliubov transformation. We set $J = 1$ for convenience. Rewriting the Pauli matrices by spin operators $\sigma_j^x = a_j^\dagger + a_j$, $\sigma_j^y = (a_j^\dagger - a_j)/\mathrm{i}$ and $\sigma_j^z = 2a_j^\dagger a_j - 1$, together with Jordan−Wigner transformation $a_j = [\exp(\mathrm{i}\pi\sum_{l=1}^{j-1}c_l^\dagger c_l)]c_j$, the Hamiltonian becomes

$$\begin{aligned} H = &-\frac{1}{2}\textstyle\sum_{j=0}^{N-1}[(c_j^\dagger c_{j+1} - c_j c_{j+1}^\dagger) + \gamma(c_j^\dagger c_{j+1}^\dagger - c_j c_{j+1}) \\ &+ \lambda(2c_j^\dagger c_j - 1)] + \frac{\mu}{2}(c_N^\dagger c_0 + c_0^\dagger c_N + \gamma c_N^\dagger c_0^\dagger \\ &+ \gamma c_0 c_N), \end{aligned} \quad (4)$$

where $\mu = \prod_{j=1}^{N} \sigma_j^z$ is the parity operator. In order to deal with the boundary term, we separate the Hamiltonian as

$$H = \frac{1+\mu}{2}H^+ + \frac{1-\mu}{2}H^-,$$
$$H^\pm = -\frac{1}{2}\sum_{j=0}^{N-1}[(c_j^\dagger c_{j+1} - c_j c_{j+1}^\dagger) + \gamma(c_j^\dagger c_{j+1}^\dagger - c_j c_{j+1}) + \lambda(2c_j^\dagger c_j - 1)], \quad (5)$$

since their even/odd parity is thereby conserved, respectively.

Now we can use the Fourier transform $c_k = \frac{e^{-i\pi/4}}{\sqrt{N}}\sum_{j=0}^{N-1} e^{-ijk}c_j$, and the Bogoliubov transformation $\gamma_k = \cos\theta_k c_k - \sin\theta_k c_{-k}^\dagger$ to complete the diagonalization, thus:

$$H^\pm = \sum_{k^\pm} \epsilon_{k^\pm}\left(\gamma_{k^\pm}^\dagger \gamma_{k^\pm} - \frac{1}{2}\right),$$
$$k^\pm = \frac{2\pi\left[n + \frac{1\pm 1}{4}\right]}{N},\ n = 0, 1, \ldots N-1, \quad (6)$$

here $\epsilon_k = [(\cos k - \lambda)^2 + \gamma^2 \sin^2 k]^{1/2}$ is the dispersion of elementary excitations. The Bogoliubov angle θ_k satisfies $\tan(2\theta_k) = \frac{\gamma \sin k}{\lambda - \cos k}$.

It has been observed in [33] that given a thermodynamical limit $N \to \infty$, we have $\langle O\rangle = \langle O\rangle_+ = \langle O\rangle_-$ for OTOC with both local and nonlocal operators in the Ising model. Here, the subscript denotes the choice of $k^\pm$ corresponding to even/odd chain length N. We confirm that this conclusion still holds for the XY model. In this paper we will use k^+ and even N for consistency.

3. Out-of-time-order correlator

Using the diagonalized Hamiltonian, we are now able to calculate the OTOC of the XY model. We consider the following term:

$$F_{\mu\nu}(l, t) = \langle \sigma_l^\mu(t)\sigma_0^\nu \sigma_l^\mu(t)\sigma_0^\nu\rangle, \quad (7)$$

where $\mu, \nu = x, y, z$. The Pauli matrices may be expressed by fermionic operators in the Majorana representation $A_j = c_j^\dagger + c_j$ and $B_j = c_j^\dagger - c_j$:

$$\sigma_j^x = (\prod_{j'<j} A_{j'}B_{j'})A_j,\ \ \sigma_j^y = -i(\prod_{j'<j} A_{j'}B_{j'})B_j,$$
$$\sigma_j^z = -A_jB_j. \quad (8)$$

All OTOCs may be expressed as the thermal average of Majorana fermion sequences. For instance, $F_{zz}(l, t) = \langle A_l(t)B_l(t)A_0B_0A_l(t)B_l(t)A_0B_0\rangle$. In terms of the thermodynamical limit, this can be computed using Wick's theorem, which turns the calculation of the long sequence into a combination of two-point correlation functions. We will use the Pfaffian method to complete the calculations numerically, with similar steps to [33].

The Pfaffian method [42, 43] can be expressed as

$$F(l, t) = \pm \mathrm{Pf}(\Phi) = \pm\sqrt{\mathrm{Det}(\Phi)}, \quad (9)$$

where the matrix Φ is skew-symmetric, i.e. $\Phi_{ii} = 0$ and $\Phi_{ij} = -\Phi_{ji}$. This form will be modified if we use 'double trick' to deal with the calculation, in which case the sign of $F(l, t)$ is not definitely positive. However, it can still be decided by requiring the 'continuity' of the OTOC, which we will elaborate below. The matrix Φ is constructed in terms of Majorana correlation functions $\Phi_{ij} = \langle X_i X_j\rangle$, where X_i is the ith element inside thermal average function $\langle X_1 X_2 \ldots\rangle$.

The basic correlation functions are $\langle A_m(t)A_n\rangle$, $\langle A_m(t)B_n\rangle$, $\langle B_m(t)A_n\rangle$, and $\langle B_m(t)B_n\rangle$, which can be derived if we know the exact diagonalized form of the Hamiltonian. Their expressions are shown in appendix.

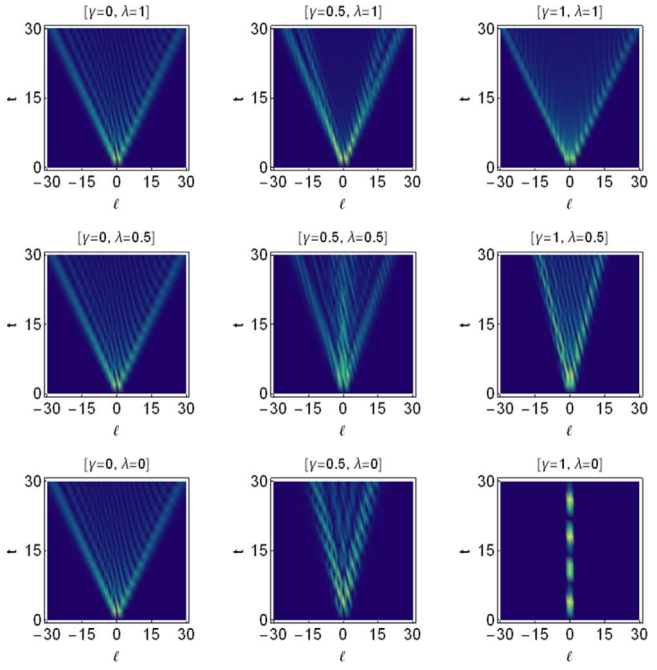

Figure 2. General evolution of C_{zz} with different choices of parameters in the XY model. We set the system size $N = 500$, inverse temperature $\beta = 0$. The space coordinate l ranges from -30 to 30. The time coordinate ranges from 0 to 30. Lighter color denotes a larger value of C_{zz}, corresponding to stronger delocalization. These images clearly show how the spreading of the operator is bounded by a 'cone structure'.

3.1. OTOC for local operators

OTOCs characterise information spreading and scrambling, in other words, the delocalization of operators. Since the behavior of many-body localized quantum systems can be revealed by the local operators, it will be interesting to study them.

For the XY model, the OTOC with local operators is C_{zz}. As shown in equation (8), operator $\sigma_j^z = -A_jB_j$ is local, since it consists of fermions located at site j only. Operators σ_j^x and σ_j^y are nonlocal because they are related to all sites of fermions before site j. Combining equations (8) and (9), we obtain

$$C_{zz}(l, t) = 1 - \mathrm{Re}[\langle (A_l(t)B_l(t)A_0B_0)^2\rangle] = 1 - \mathrm{Re}\sqrt{\mathrm{Det}(\Phi_{zz})}. \quad (10)$$

With the help of the Pfaffian trick, we can compute this quantity numerically. The results in figure 2 illustrate how the

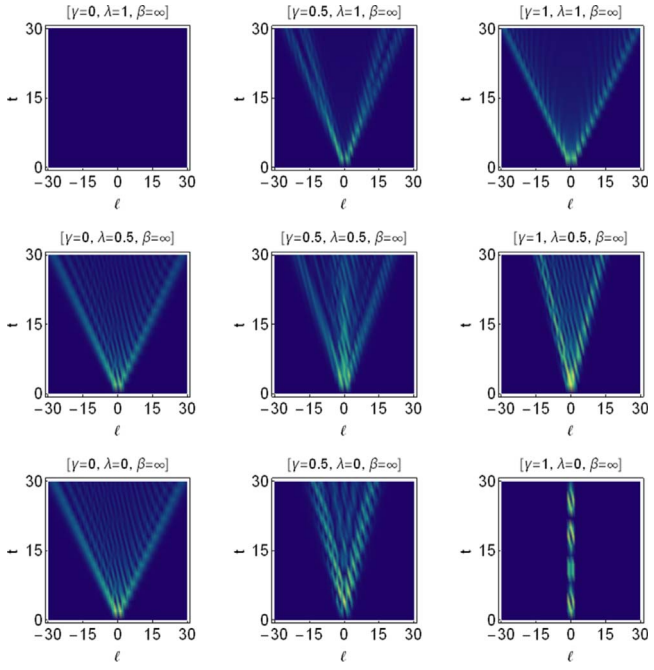

Figure 3. The evolution of C_{zz} at zero temperature $T = 1/\beta = 0$ with other configurations, as in figure 2. This shows that only the model where ($\gamma = 0$, $\lambda = 1$) displays vanishing C_{zz}. All other models are not sensitive to temperature.

parameters (γ, λ) affect the evolution of the OTOC and the spreading velocity of the butterfly effect. Here, we choose the system size $N = 500$ and $\beta = 0$. The lighter color in the figure denotes stronger $C(t)$. Thus we can observe how the OTOC spreads.

Several interesting properties can be observed from these results. Firstly, the cone structure indicates a binding of the butterfly effect, except in the model where $\gamma = 1$, $\lambda = 0$, which corresponds to the quantum Ising chain without external magnetic field. The $C(t)$ of this model is always zero, except for sites $l = 0$ and ± 1. This indicates that the operators do not spread there. This may be further illustrated by considering the HBC formula as follows:

$$W(t) = \sum_{n=0}^{\infty} \frac{(it)^n}{n!} L_n(W) = W + it[H, W] + \frac{(it)^2}{2!}[H, [H, W]] + ... \quad (11)$$

When $\gamma = 1$, $\lambda = 0$, the commutator $[W(l, t), V(0)] = [\sigma_l^z(t), \sigma_0^z]$ vanishes for all sites except $l = 0, \pm 1$. Therefore $C(l, t) \equiv \frac{1}{2}\langle|[W(l, t), V(0)]|^2\rangle$ also vanishes.

Secondly, the butterfly effect of the spin chains where ($\gamma = 1$, $\lambda = 1$) and ($\gamma = 0$, $0 < \lambda < 1$) always satisfy $v_B = 1$. In the latter case, the OTOC is not influenced by the magnetic field λ if $\gamma = 0$ and $\beta = 0$. Nevertheless, the other positions display a narrower cone structure. This indicates that their speed of operator spreading is slower, and that the velocity v_B depends on γ and λ. We can conclude that the existence of anisotropy will affect the speed of operator spreading. For models with a weak magnetic field, this will cause a reduction in speed.

Thirdly, by comparing figure 3 with figure 2, we note that temperature has a negligible effect on OTOCs with local operators, except for the model where ($\gamma = 0$, $\lambda = 1$). This model displays vanishing OTOC when the temperature falls to zero. The reason for this phenomenon is currently unclear.

There is a conjecture that around the wavefront of information spreading, the wavefront of $C(t)$ can be described by the universal form (2). To verify this conjecture in the XY model, we calculate the wavefront of C_{zz} along fixed-velocity rays. The results are shown in figure 4.

We posit that

$$C(t) = const. \times \exp(-\lambda_L(v)t). \quad (12)$$

If the universal form indeed holds in the XY model, we should obtain the relation

$$\mathrm{Log}[C(t)] = -\lambda_L(v)t + \text{const.}, \quad \lambda_L(v) \sim (v - v_B)^{1+1/2}, \quad (13)$$

as $p = 1/2$ for XY model.

In figure 4, we use time t and $\mathrm{Log}[C_{zz}]$ as coordinates, where the fixed velocity $v = 1.1$, 1.2, and 1.5. Then we use form $-\lambda_L(v)t + const.$ to fit the numerical results. In the insets, the values of $\lambda_L(v)$ are extracted by fitting the numerical data. The power law relations are checked. For example, in the top picture, the coordinates of three points are (1.1, 0.38), (1.2, 0.54), and (1.5, 1.14), which fits function $\lambda_L(v) = 1.82(v - 0.75)^{3/2}$ quite well. In addition, we can see from figure 2 that the butterfly velocity of model ($\gamma = 0.5$, $\lambda = 0.5$) is indeed $v_B \approx 0.75$. The other two figures also support this relation quite well. We conclude that for OTOC with local operators, the universal form is supported by XY model. On the other hand, this result also supports our former conclusion that v_B depends on γ and λ.

Now we consider the time evolution of C_{zz} at fixed sites. It will tell us exactly how the local operators will behave. Two meaningful areas must be considered: the early time and the long time. The results of models at four typical points are illustrated in figure 5 with sites $l = 1$, 2, 3, 4. It is clear that for the early time, C_{zz} is vanishing at ($\gamma = 1$, $\lambda = 0$), when $l > 1$. We can also observe power law t^{4l-2} at ($\gamma = 1$, $\lambda = 1$) and at t^{2l} for the remaining models. These behaviors can be understood by means of the HBC formula. Since t is small for early time, the description by HBC expansion remains quite accurate. Note that the lowest order of t, which makes $C(t)$ nonzero, is decided by the lowest order of $L_n(W)$ that satisfies $[L_n(W), V] \neq 0$. To be specific, the Hamiltonian of the XY model may be divided into six different types by selecting different values of γ and λ. They are (1). $\sigma^x\sigma^x$, (2). $\sigma^y\sigma^y$, (3). $\sigma^x\sigma^x+\sigma^z$, (4). $\sigma^y\sigma^y+\sigma^z$, (5). $\sigma^x\sigma^x+\sigma^y\sigma^y$, (6). $\sigma^x\sigma^x+\sigma^y\sigma^y+\sigma^z$. For zz OTOCs, the $\sigma^x\sigma^x$ and $\sigma^y\sigma^y$ exhibit the same behavior. Therefore, we can observe that there are four kinds of behaviors. We know that type (1) and (2) have vanishing $C(t)$. For type (3), however, we see that

$$L_1(\sigma_0^z) = [H, \sigma_0^z] \sim \sigma_0^y\sigma_1^x, \quad L_2(\sigma_0^z) \sim [H, \sigma_0^y\sigma_1^x] \sim \sigma_0^y\sigma_1^y, \quad L_3(\sigma_0^z) \sim [H, \sigma_0^y\sigma_1^y] \sim \sigma_0^y\sigma_1^z\sigma_2^x \ \ldots . \quad (14)$$

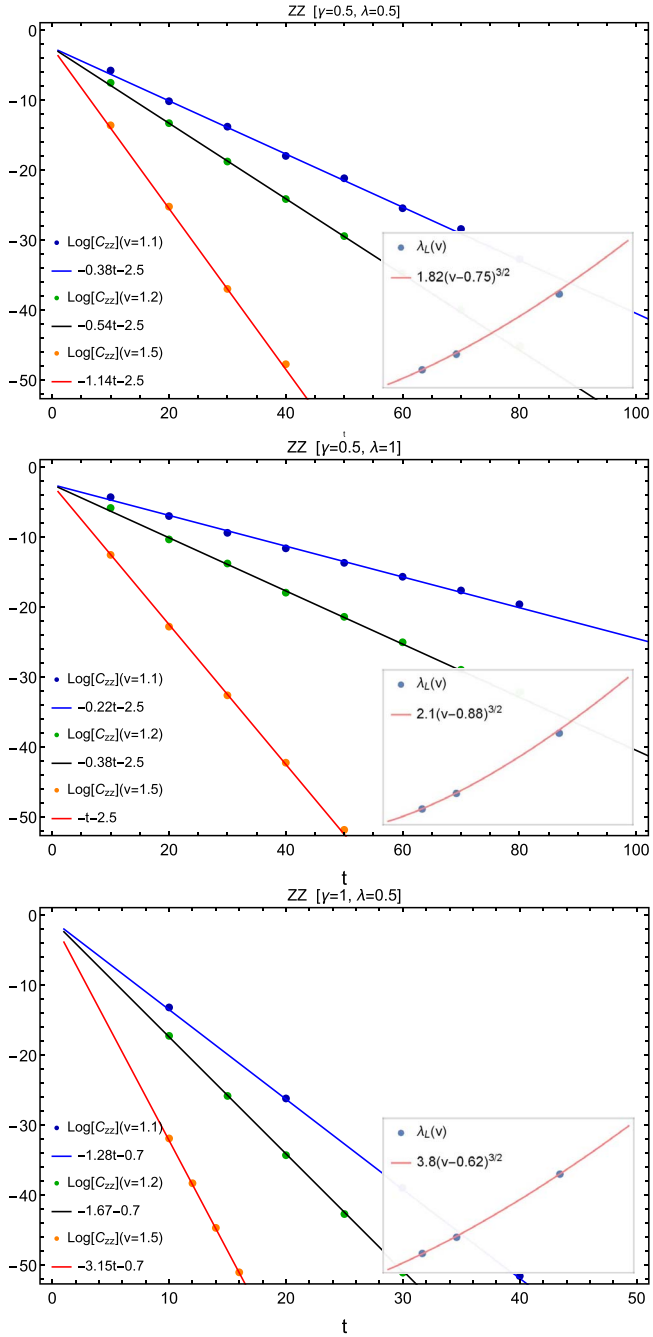

Figure 4. Fitting of the universal form and numerical data of C_{zz}. We select three models with different v_B to confirm whether the conjecture holds in the XY model. The dots represent numerical data from the OTOC along velocity-fixed rays, where $v = 1.1$, 1.2, and 1.5, respectively. The solid lines are fitting forms of $-at + b$. Coefficient a is the velocity-dependent Lyapunov exponents $\lambda_L(v)$ that we need to extract. The insets show the three sets of extracted data fitted by $\sim(v - v_B)^{1+p}$. We note that the numerical data fits quite well.

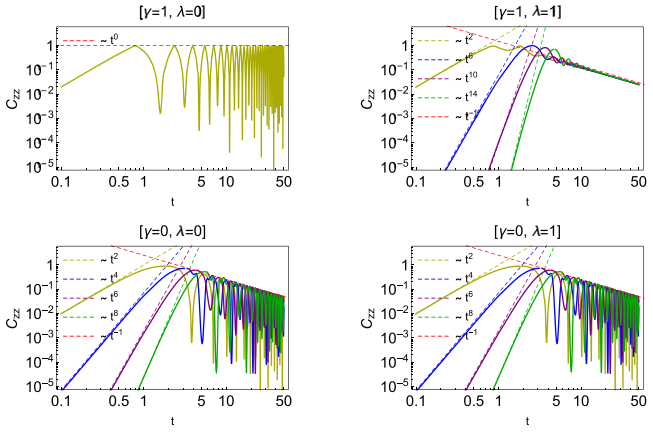

Figure 5. Time evolution of C_{zz} with four typical models. Yellow, blue, purple, and green lines correspond to fixed locations $l = 1$, 2, 3, 4, respectively. C_{zz} at ($\gamma = 1$, $\lambda = 0$) vanishes for $l > 1$. The dashed lines are used to show power law fitting. We can see clearly from the figures that these models show t^{4l-2} and t^{2l} power law growth at early time, and t^{-1} decay at late-time, independent of site l.

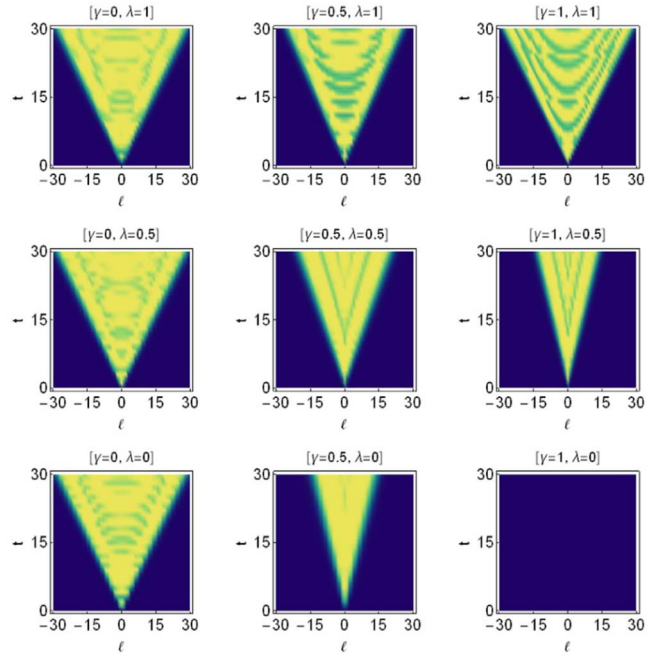

Figure 6. General evolution of C_{xx} with different choices of parameters in the XY model. We set system size $N = 100$, inverse temperature $\beta = 0$. Coordinates are given as space ranges from -30 to 30, time ranges from 0 to 30, respectively. Lighter color indicates a larger value of C_{xx}, corresponding to stronger delocalization. These images show similar light cone binding for the different models, but some differences may be observed, as compared with local operators inside the light cone: relatively speaking, they appear more scrambled.

The lowest order $[L_n(\sigma_0^z), \sigma_l^z] \neq 0$ and $[\sigma_0^z(t), \sigma_l]$ shows t^{2l-1} power law growth. Thus $C(t) = \frac{1}{2}\langle|[\sigma_0^z(t), \sigma_l]|^2\rangle$ evolves as t^{4l-2}. The early-time behaviors of other types may also be checked in a similar fashion. Note that type (5) and type (6) show the same t^{2l} growth behavior. This is because when x and y components exist at the same time, their behavior will dominate. Overall, we conclude that the early-time behaviors of C_{zz} can be separated into three types: t^{4l-2} at ($\gamma = 1$, $\lambda \neq 0$), t^{2l} at $\gamma \neq 1$, and when $l > 1$, vanishing will occur at ($\gamma = 1$, $\lambda = 0$).

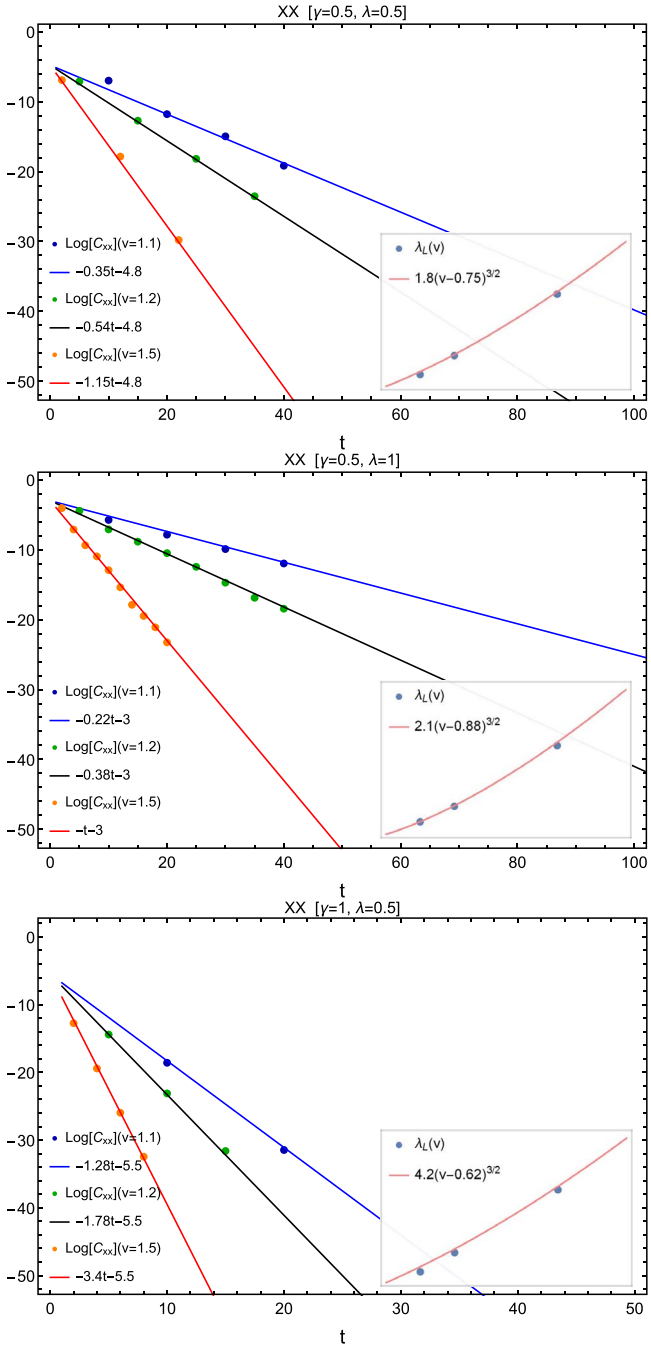

Figure 7. Fitting results for the universal form and numerical data of C_{xx}. We select three models with different v_B ; note that all other models of OTOC with nonlocal operators have also been verified. The outside dots represent numerical data obtained by calculating the OTOC along velocity-fixed rays where $v = 1.1$, 1.2, and 1.5 respectively. The solid lines are fitting forms of $-at + b$, and a is the velocity-dependent Lyapunov exponents $\lambda_L(v)$ that we need to extract. The inset shows how these three sets of extracted data fitted with $\sim(v - v_B)^{1+p}$ as a function of v. We observe that the numerical data fits quite well.

Next, we examine the late-time aspect of C_{zz}. As exhibited in figure 5, all models decay as t^{-1}, independent of γ, λ, site l, and temperature. This behavior may be understood by means of the stationary phase approximation of fermionic

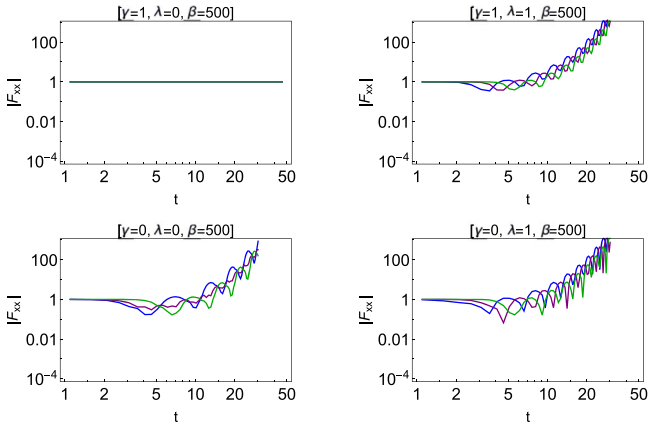

Figure 8. Late-time behavior of $|F_{xx}|$ at low temperature $\beta = 500$. Blue, purple, and green lines correspond to fixed locations $l = 2$, 3, and 4 respectively. The OTOC is observed to be divergent at late-time.

Table 1. Summary of early-time power law growth of OTOCs with both local and nonlocal operators in the XY model.

	(1, 1)	(0, 1)	(1, 0)	(0, 0)
C_{xx}	t^{4l+2}	$t^{2l+1+(-1)^l}$	—	$t^{2l+1+(-1)^l}$
C_{xy}	t^{4l}	$t^{2l+1-(-1)^l}$	—	$t^{2l+1-(-1)^l}$
C_{yy}	t^{4l-2}	$t^{2l+1+(-1)^l}$	—	$t^{2l+1+(-1)^l}$
C_{xz}	t^{4l}	t^{2l}	—	t^{2l}
C_{yz}	t^{4l-2}	t^{2l}	—	t^{2l}
C_{zz}	t^{4l-2}	t^{2l}	$t^0(l=1)$	t^{2l}

correlation functions, i.e. when $t \to \infty$, we obtain [33]

$$C_{zz}(l, t) \sim (1 - \langle A_0 B_0\rangle^2)\frac{2}{\pi|\epsilon''_\pi|t}, \tag{15}$$

here, ϵ''_π is the second derivative of ϵ_k with $k = \pi$.

3.2. OTOC with nonlocal operators

There are five types of OTOC with nonlocal operators in the XY model: i.e. F_{xx}, F_{yy}, F_{xy}, F_{xz}, and F_{yz}. However, since the operators σ_j^x and σ_j^y change the fermion parity, their Heisenberg evolution cannot simply obtained from $A_j(t)$ and $B_j(t)$. Following the method used in [33, 44], we will use the 'double trick' to calculate the OTOC. Define quantity

$$\Gamma_{\mu\nu}(j, t) \equiv \langle(\sigma^\mu_{\frac{N}{2}}(t)\sigma^\mu_{N-j}(t)\sigma^\nu_0\sigma^\nu_{\frac{N}{2}-j})^2\rangle, \tag{16}$$

for large enough N. Invoking Lieb-Robinson bound and cluster property [44], we obtain

$$\begin{aligned}\Gamma_{\mu\nu}(j, t) &\approx \langle(\sigma^\mu_{\frac{N}{2}}(t)\sigma^\nu_{\frac{N}{2}-j})^2\rangle\langle(\sigma^\mu_{N-j}(t)\sigma^\nu_0)^2\rangle \\ &= F_{\mu\nu}(j, t)F_{\mu\nu}(-j, t) = F^2_{\mu\nu}(j, t),\end{aligned} \tag{17}$$

here, $F_{\mu\nu}(j, t) = F_{\mu\nu}(-j, t)$ due to mirror symmetry.

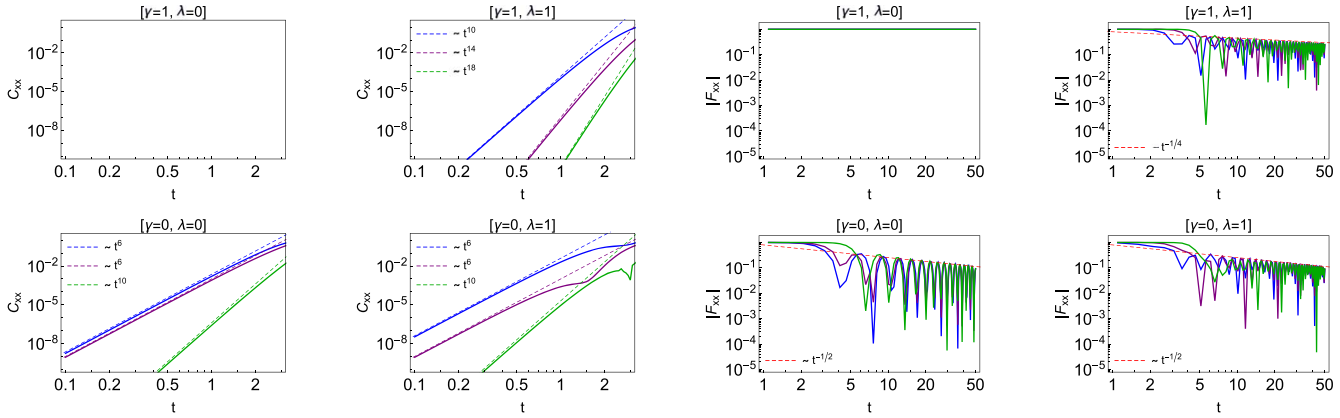

Figure 9. Early- and late-time evolution of xx OTOC with four sets of parameters and fixed location $l = 2$, 3, and 4 (blue, purple, and green lines, respectively).

Taking xx OTOC as an example, quantity $\Gamma_{xx}(j, t)$ can be expressed as

$$\Gamma_{xx}(j, t) = \Big\langle [(\prod_{j'=\frac{N}{2}}^{N-j-1} B_{j'}(t)A_{j'+1}(t) \times (\prod_{j'=0}^{\frac{N}{2}-j-1} B_{j'}A_{j'+1})]^2 \Big\rangle. \quad (18)$$

We can use the Pfaffian method to calculate this. We construct a matrix Φ_{xx} of dimension $4(N-2j) \times 4(N-2j)$. Then $F_{xx}(j, t)$ can be calculated as

$$F_{xx}(j, t) = \pm\sqrt{|\mathrm{Pf}(\Phi_{xx})|} = \pm[\mathrm{Det}(\Phi_{xx})]^{\frac{1}{4}}. \quad (19)$$

Since the quantity is doubled, we do not know the sign of it directly. However, this can be recovered by requiring the 'continuity' of $F_{xx}(j, t)$. More specifically, there is a critical rule for all the points on site j and time t: on the premise of turning least directions, choose closest distance. With this rule we can check how the curve is finally organized with all the points from calculation. It should be noted that when $j > vt$, $F_{xx} \to 1$, due to the existence of cone structure. OTOCs with other operators may be calculated in the same way. Combining equations (8) and (17) gives

$$\Gamma_{xy}(j, t) = \Big\langle [(\prod_{j'=\frac{N}{2}}^{N-j-1} B_{j'}(t)A_{j'+1}(t) \times (\prod_{j'=0}^{\frac{N}{2}-j-1} A_{j'}B_{j'+1})]^2 \Big\rangle, \quad (20)$$

$$\Gamma_{xz}(j, t) = \langle [(\prod_{j'=\frac{N}{2}}^{N-j-1} B_{j'}(t)A_{j'+1}(t) \times A_0 A_{N/2-l} B_0 B_{N/2-l}]^2 \rangle. \quad (21)$$

Γ_{yy} and Γ_{yz} can also be constructed in the same way.

The general behavior of C_{xx} with system size $N = 100$ and $\beta = 0$ is illustrated in figure 6. Other $C(t)$s with different operators show similar behaviors, so we will not show them here. We can see that while $C(t)$ in figure 3 is vanishing at $(\gamma = 0, \lambda = 1)$, it does not vanish with nonlocal operators. From these figures, we see that the butterfly velocity is the same as for local operators. This indicates that the butterfly velocity only depends on the model, not the operators, in OTOC function. Moreover, scrambling is observed for all sites inside the 'light cone'. When $\gamma = 0$, $\beta = 0$, λ has tiny effect on the OTOC. The observation of scrambling in OTOCs with nonlocal operators illustrates their main differences compared with local operators. This can easily be understood, since nonlocal operators possess nonlocal information about operators, which leads to delocalization once they spread inside the light cone.

Table 2. Summary of long-time power law growth of OTOC for both local and nonlocal operators in the XY model.

	(1, 1)	(0, 1)	(1, 0)	(0, 0)
$\lvert F_{xx}\rvert$	$t^{-1/4}$	$t^{-1/2}$	—	$t^{-1/2}$
$\lvert F_{xy}\rvert$	t^{-2}	$t^{-3/2}$	—	$t^{-1/2}$
$\lvert F_{yy}\rvert$	t^{-3}	$t^{-1/2}$	—	$t^{-1/2}$
$\lvert F_{xz}\rvert$	t^{0}	t^{-2}	—	t^{-2}
$\lvert F_{yz}\rvert$	t^{0}	t^{-2}	—	t^{-2}
C_{zz}	t^{-1}	t^{-1}	$t^0(l=1)$	t^{-1}

Knowing that the butterfly velocity of the different operators remains unchanged within the same model, we further examine whether the universal form regarding wavefront behavior holds in the case of nonlocal operators. Here we only show the results C_{xx} due to space contstraints, but we have confirmed that all nonlocal $C(t)$ support the conjecture quite well. The results are illustrated in figure 7. We can clearly see the fitting results of numerical data in the insets.

The evolution of OTOCs with nonlocal operators can also be analyzed, including their early-time and long-time power law behaviors. With regard to early-time observations, detailed plots are included in figures 9–13, and summarize the results in table.1. Note that since $l = 1$ is no longer a special case for nonlocal operators, we only plot results of $l = 2$, 3 , and 4, for clarity. Here, the sign of the OTOC is no longer a problem; since $C(t)$ are relatively close to 0 at early time, the sign of $|F(t)|$ must be positive. These results are actually not beyond our expectation because all of them agree with the HBC formula. Thus, this aspect requires no further consideration.

It should be noted, however, that long-time behavior is in some ways more subtle. In [33], the author found that for a quantum Ising chain at the critical point, $|F_{xx}(t)|$ exhibits

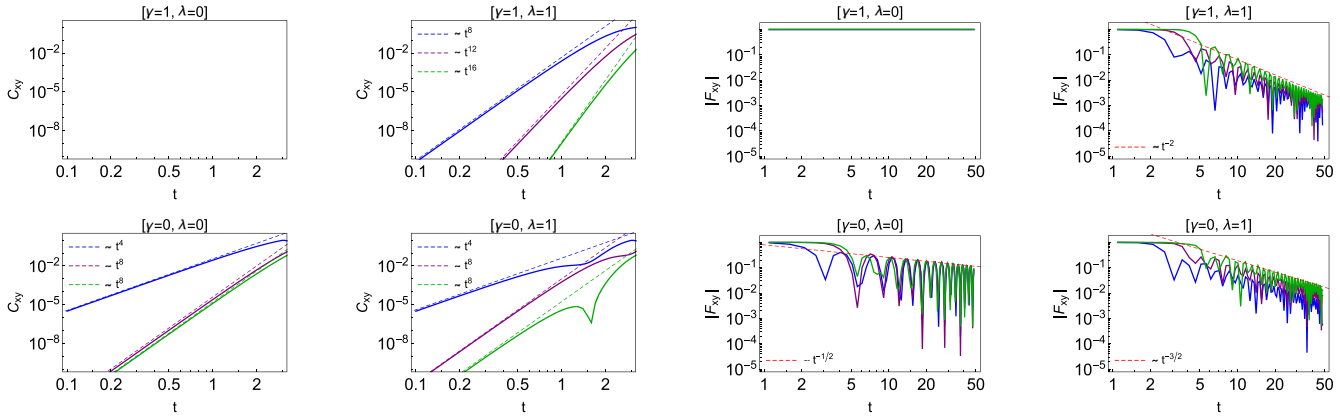

Figure 10. Early- and late-time evolution of xy OTOC with four sets of parameters and fixed location $l = 2$, 3, and 4 (blue, purple, and green lines, respectively).

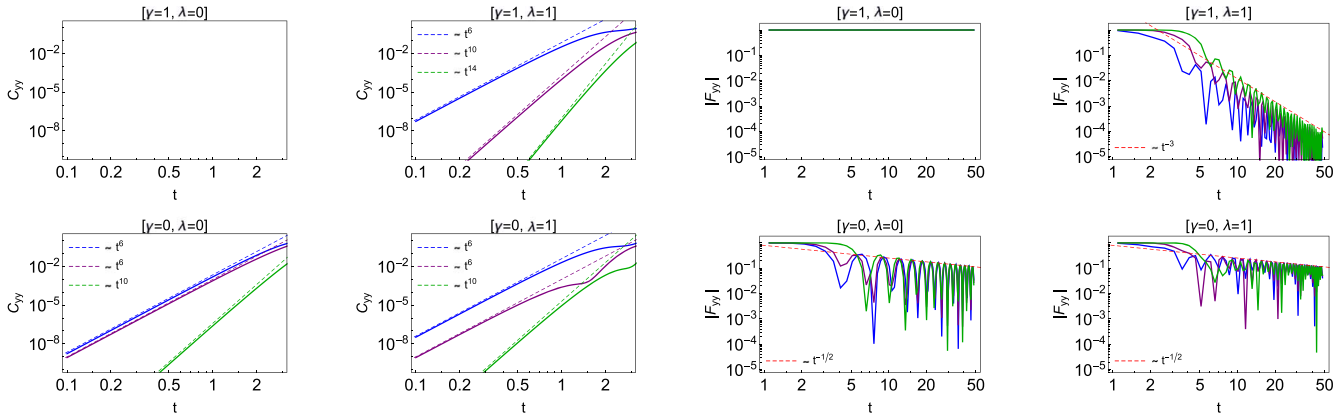

Figure 11. Early- and late-time evolution of yy OTOC with four sets of parameters and fixed location $l = 2$, 3, and 4 (blue, purple, and green lines, respectively).

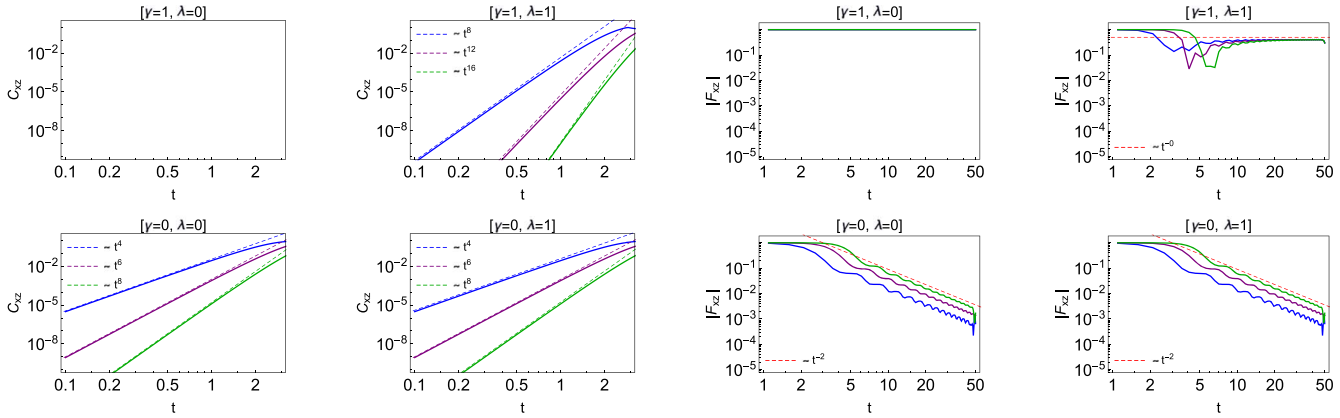

Figure 12. Early- and late-time evolution of xz OTOC with four sets of parameters and fixed location $l = 2$, 3, and 4 (blue, purple, and green lines, respectively).

nontrivial $t^{-1/4}$ decay at long-time. Here, we confirm this result, and examine further long-time behaviors in other regions. The results are shown in figures 9–13 and table 2. Surprisingly, they show quite different power law behaviors for different selections of γ and λ. We know that at late-time, $|F(t)|$ with nonlocal operators approach 0, which indicates that $C(t)$ is appoaching saturation value 1. Thus, the power law behaviors indicate that different operators will exhibit different rates of saturation. In particular $|F_{xz}(t)|$ and $|F_{yz}(t)|$, which describe how nonlocal operators and local operators interact with each other, show no decay at the critical point. This observation indicates that for these two kinds of OTOC,

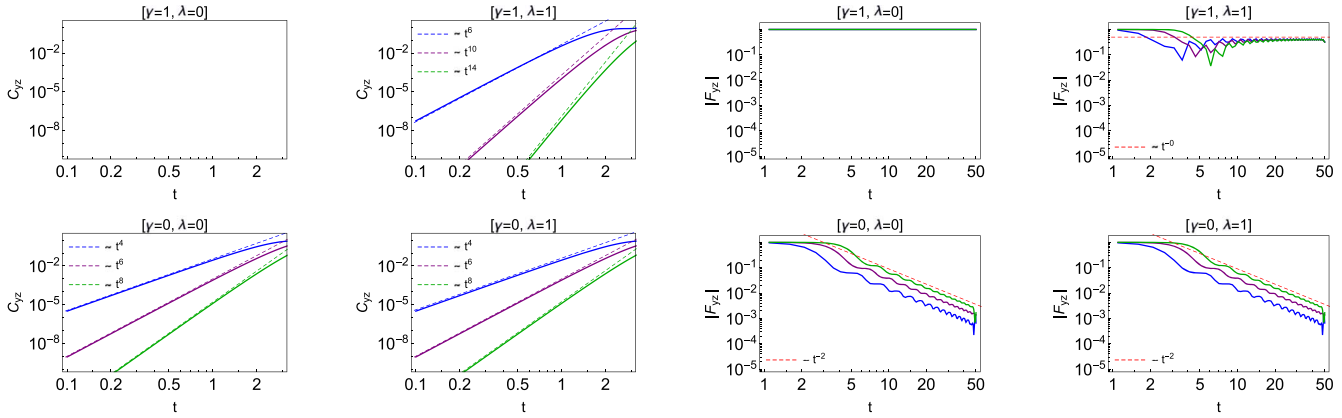

Figure 13. Early- and late-time evolution of yz OTOC with four sets of parameters and fixed location $l = 2$, 3, and 4 (blue, purple, and green lines, respectively).

$C(t)$ will be constant at very long time, and will not grow at all.

Moreover, our results appear to be independent of location l when $\beta = 0$. However, if we set β to a bigger value, the pattern of the OTOC becomes quite complex. Some results of $|F_{xx}|$ are shown in figure 8. Divergence can be observed at late-time. The reason for this is currently unclear, as we used numerical method rather than analytical form to complete the calculations. As a result, we have been unable to obtain a universal description of the long-time behaviors of OTOCs with nonlocal operators, but we do hope that our calculations will contribute towards achieving the final form.

4. Discussion and conclusion

The study of OTOCs in integrable systems is a relatively new area of research, and may reveal a great deal of interesting information about how operators evolve in such systems, and how scrambling happens. In this work we mainly focus on the behaviors of OTOCs in the XY model, including early time, long time, and wavefront aspects, together with an examination of the conjectured universal form (2). Careful calculation and analysis reveals some interesting points relating to OTOCs in this system. We found that the butterfly velocity in the XY model depends on its anisotropy parameter γ and magnetic field λ, but is independent of the locality of the operators in the OTOC. Based on this observation, we proved that for all kinds of OTOC, with all choices of parameters in the XY model, the conjectured form (2) regarding wavefront behavior holds true. Therefore, it is indeed a viable description of OTOCs around wavefront ($v > v_B$), at least insofar as it relates to the XY model.

Furthermore, we conducted a comprehensive study of the time and space evolution of OTOCs with both local and nonlocal operators in the XY model. We find some interesting points about their general behavior: (1) When $\gamma = \beta = 0$, OTOCs with local operators are independent of the external magnetic field λ; (2) For the noncritical point $\gamma = 0$, $\lambda = 1$, OTOCs with local operators vanish when the temperature tends to zero. This phenomenon does not occur with other typical sets of parameters. In addition to these results, the early-time, and long-time evolution of OTOCs at fixed locations have also been studied. We found that while early-time behavior agrees with the power law results of the HBC formula, the long-time behaviors exhibit nontrivial saturation rates for different operators and models. These are independent of location l when $\beta = 0$. However, when temperature decreases, their behaviors become very complex. This is not easy to analyze by means of numerical calculation. In addition, OTOCs with both local and nonlocal operators, i.e. $|F_{xz}|$ and $|F_{yz}|$ show t^0 at long time. Their long-time evolutions are constant, rather than approaching 0 as other systems do.

Overall, we have studied many aspects of OTOCs in the XY model, and provide some evidence to support the conjecture regarding information spreading around wavefronts. Further research is required in order to better understand the underlying values of these observations and conclusions, which may be explored in future experiments. Equally, further analysis of OTOCs in other systems is also required in order to arrive at a more profound understanding of their behaviour in both chaotic and integrable systems.

Acknowledgments

We thank Peng-Cheng Li for helpful discussions. This work is funded by the China Postdoctoral Science Foundation. Cheng-Yong Zhang is supported by NSFC Grant No. 11 947 067.

Appendix. Majorana two-point correlation functions

Following the definition of the Majorana representation, we obtain:

$$\langle A_m(t)A_n\rangle = \langle (c_m^\dagger(t) + c_m(t))(c_n^\dagger + c_n)\rangle, \tag{A1}$$

$$\langle A_m(t)B_n\rangle = \langle (c_m^\dagger(t) + c_m(t))(c_n^\dagger - c_n)\rangle, \tag{A2}$$

$$\langle B_m(t)A_n\rangle = \langle (c_m^\dagger(t) - c_m(t))(c_n^\dagger + c_n)\rangle, \tag{A3}$$

$$\langle B_m(t)B_n\rangle = \langle (c_m^\dagger(t) - c_m(t))(c_n^\dagger - c_n)\rangle. \tag{A4}$$

Next, by means of the Fourier transformation $c_j = \frac{e^{i\pi/4}}{\sqrt{N}}\sum_k e^{ijk}c_k$, and the Bogoliubov transformation $c_k = \cos\theta_k\gamma_k + \sin\theta_k\gamma^\dagger_{-k}$, it becomes straightforward to expand the above forms in momentum space. Finally, we obtain

$$\langle A_m(t)A_n\rangle = \frac{1}{N}\sum_k\Big[\cos(\epsilon_k t) - i\sin(\epsilon_k t)\tanh\frac{\beta\epsilon_k}{2}\Big]e^{i(m-n)k}, \tag{A5}$$

$$\langle A_m(t)B_n\rangle = \frac{1}{N}\sum_k\Big[\cos(\epsilon_k t)\times\tanh\frac{\beta\epsilon_k}{2} - i\sin(\epsilon_k t)\Big]e^{2i\theta_k}e^{i(m-n)k}, \tag{A6}$$

$$\langle B_m(t)A_n\rangle = -\frac{1}{N}\sum_k\Big[\cos(\epsilon_k t)\tanh\frac{\beta\epsilon_k}{2} - i\sin(\epsilon_k t)\Big]e^{-2i\theta_k}e^{i(m-n)k}, \tag{A7}$$

$$\langle B_m(t)B_n\rangle = -\frac{1}{N}\sum_k\Big[\cos(\epsilon_k t) - i\sin(\epsilon_k t)\tanh\frac{\beta\epsilon_k}{2}\Big]e^{i(m-n)k}. \tag{A8}$$

ORCID iDs

Cheng-Yong Zhang https://orcid.org/0000-0002-1017-3234

References

[1] Shenker S H and Stanford D 2014 *JHEP* **03** 067
[2] Maldacena J, Shenker S H and Stanford D 2016 *JHEP* **08** 106
[3] Sekino Y and Susskind L 2008 *JHEP* **10** 065
[4] Lashkari N, Stanford D, Hastings M, Osborne T and Hayden P 2013 *JHEP* **04** 022
[5] Huang Y, Zhang Y and Chen X 2017 *Ann. Phys., Lpz.* **529** 1600318
[6] Chen X, Zhou T, Huse D A and Fradkin E 2017 *Ann. Phys., Lpz.* **529** 1600332
[7] Slagle K, Bi Z, You Y-Z and Xu C 2017 *Phys. Rev.* **B95** 165136
[8] Fan R, Zhang P, Shen H and Zhai H 2017 *Sci. Bull.* **62** 707–11
[9] Deng D-L, Li X, Pixley J H, Wu Y-L and das Sarma S 2017 *Phys. Rev.* B **95** 024202
[10] Swingle B, Bentsen G, Schleier-Smith M and Hayden P 2016 *Phys. Rev.* A **94** 040302
[11] Zhu G, Hafezi M and Grover T 2016 *Phys. Rev.* A **94** 062329
[12] Kaufman A M, Tai M E, Lukin A, Rispoli M, Schittko R, Preiss P M and Greiner M 2016 *Science* **353** 794
[13] Gärttner M 2017 *Nat. Phys.* **13** 781
[14] Landsman K A, Figgatt C, Schuster T, Linke N M, Yoshida B, Yao N Y and Monroe C 2019 *Nature* **567** 61–5
[15] Lukin A, Rispoli M, Schittko R, Tai M E, Kaufman A M, Choi S, Khemani V, Léonard J and Greiner M 2019 *Science* **364** 256–60
[16] Xu S and Swingle B 2020 *Nat. Phys.* **16** 199–204
[17] Khemani V, Huse D A and Nahum A 2018a *Phys. Rev.* B **98** 144304
[18] Nahum A, Vijay S and Haah J 2018 *Phys. Rev.* X **8** 021014
[19] von Keyserlingk C, Rakovszky T, Pollmann F and Sondhi S 2018 *Phys. Rev.* X **8** 021013
[20] Khemani V, Vishwanath A and Huse D A 2018 *Phys. Rev.* X **8** 031057
[21] Lin C-J and Motrunich O I 2018 *Phys. Rev.* B **98** 134305
[22] Jian S-K and Yao H 2018 arXiv:1805.12299
[23] Sachdev S and Ye J 1993 *Phys. Rev. Lett.* **70** 3339
[24] Gu Y, Qi X-L and Stanford D 2017 *JHEP* **05** 125
[25] Roberts D A, Stanford D and Susskind L 2015 *JHEP* **03** 051
[26] Stanford D 2016 *JHEP* **10** 009
[27] Roberts D A and Stanford D 2015 *Phys. Rev. Lett.* **115** 131603
[28] Chowdhury D and Swingle B 2017 *Phys. Rev.* **D96** 065005
[29] Patel A A, Chowdhury D, Sachdev S and Swingle B 2017 *Phys. Rev.* X **7** 031047
[30] Shen H, Zhang P, Fan R and Zhai H 2017 *Phys. Rev.* B **96** 054503
[31] Sun Z-H, Cai J-Q, Tang Q-C, Hu Y and Fan H 2020 *Ann. Phys., Lpz.* **2020** 1900270
[32] Dra B and Moessner R 2017 *Phys. Rev. Lett.* **119** 026802
[33] Lin C-J and Motrunich O I 2018 *Phys. Rev.* B **97** 144304
[34] Byju S, Lochan K and Shankaranarayanan S 2018 arXiv:1808.07742
[35] Jonathon R and Erik S 2019 *Phys. Rev.* B **99** 054205
[36] McGinley M, Nunnenkamp A and Knolle J 2019 *Phys. Rev. Lett.* **122** 020603
[37] Kukuljan I, Grozdanov S and Prosen T 2017 *Phys. Rev.* **B96** 060301
[38] Lieb E H, Schultz T and Mattis D 1961 *Annals Phys.* **16** 407
[39] Sachdev S 2011 *Quantum Phase Transitions* (Cambridge: Cambridge University Press)
[40] Franchini F 2017 *An Introduction to Integrable Techniques for One-dimensional Quantum Systems* vol. 940 (Berlin: Springer)
[41] Latorre J I, Rico E and Vidal G 2004 *Quant. Inf. Comput.* **4** 48
[42] Lieb E H 1968 *J. Comb. Theory* **5** 313
[43] Bravyi S and König R 2012 *Commun. Math. Phys.* **316** 641
[44] McCoy B M, Barouch E and Abraham D B 1971 *Phys. Rev.* A **4** 2331